

A Generalized Spectral-Domain Green's Function for Multilayer Dielectric Substrates with Application to Multilayer Transmission Lines

NIROD K. DAS AND DAVID M. POZAR, MEMBER, IEEE

Abstract—A generalized full-wave Green's function completely defining the field inside a multilayer dielectric structure due to a current element arbitrarily placed between any two layers is derived in two-dimensional spectral-domain form. It is derived by solving a “standard” form containing the current element with two substrates on either side of it, and using an iterative algorithm to take care of additional layers. Another iterative algorithm is then used to find the field in any layer in terms of the field expressions in the two layers of the “standard” form. The locations of the poles of the Green's function are predicted, and an asymptotic form is derived along with the asymptotic limit, by use of which the multilayer Green's function can be used in numerical methods as efficiently as the single-layer grounded-dielectric-substrate Green's function. This Green's function is then applied to a few multilayer transmission lines for which data are not found in the literature to date.

I. INTRODUCTION

SPETRAL-DOMAIN Green's functions are extensively used for analysis of microstrip antennas and planar transmission lines [1]–[7]. In [1], the Green's function for one-layer grounded dielectric substrate is used for analysis of rectangular microstrip patch antennas. In [2], similar Green's function for two dielectric layers with the same dielectric constant are used to study microstrip antennas with a protective dielectric cover. In both [1] and [2], the two-dimensional Green's function is derived by solving Maxwell's equations in the spectral domain with suitable boundary conditions at all interfaces. Extending this procedure for multiple layers (dielectric or ground planes), which is necessary for a number of applications, becomes too complicated. In [8], the spectral-domain Green's function for multiple layers is presented in one dimension to solve transmission-line structures; it uses an equivalent transmission-line model along with some simple coordinate transformations. Solutions of multilayer transmission-line structures in the spectral domain are also presented in different forms in [9] and [10].

In this paper, a generalized spectral-domain Green's

function in two dimensions is derived in a way similar to [1] and [2] in terms of suitable components of the vector electric and magnetic potentials. With these vector potentials, the boundary conditions are simplified into equivalent transmission-line problems in the spectral domain, as in [8]. The solutions are then simplified to solving a “standard” form containing only two layers of dielectric substrates, and computing the effect of all other layers by the use of an iterative algorithm. Iterative algorithms are derived (i) to compute the contribution of all other layers and (ii) to compute the Green's function in a different layer on the basis of knowledge of the Green's function in a layer adjacent to the exciting current element. The behavior of this Green's function is analyzed in detail from the point of view of using it in a computationally efficient manner. Locations of the TE and TM surface wave poles are predicted, and methods to locate them accurately are demonstrated. The complexity of computing the Green's function increases in proportion to the number of layers; thus, it may not be numerically efficient in moment-method solutions of complex structures. An asymptotic form is obtained in a very simple way, however, which can be as efficient in its numerical evaluation as a single-layer grounded-dielectric-substrate Green's function. The threshold beyond which the asymptotic form is valid is given.

This Green's function is then used to study a number of planar transmission-line structures. Using this Green's function, the propagation constant of a transmission-line structure is found as the solution to an integral equation. The expression for characteristic impedance is also obtained. Practical transmission-line-structure problems, such as the effect of a small air gap introduced while fabricating striplines and covered microstrip lines by overlapping two dielectric substrates, are studied. Characteristics of covered microstrip lines with a dielectric cover of different dielectric constant, and striplines with two different dielectric substrates are also obtained. Dispersion characteristics of some multilayer TEM-like transmission-line structures are given for a range of frequencies from 1.0 to 10.0 GHz. Data are given for standard available substrate

Manuscript received July 30, 1986; revised October 27, 1986. This work was supported in part by the National Science Foundation under Grant ECS 8352325.

The authors are with the Department of Electrical and Computer Engineering, University of Massachusetts, Amherst, MA 01003.

IEEE Log Number 8612439.

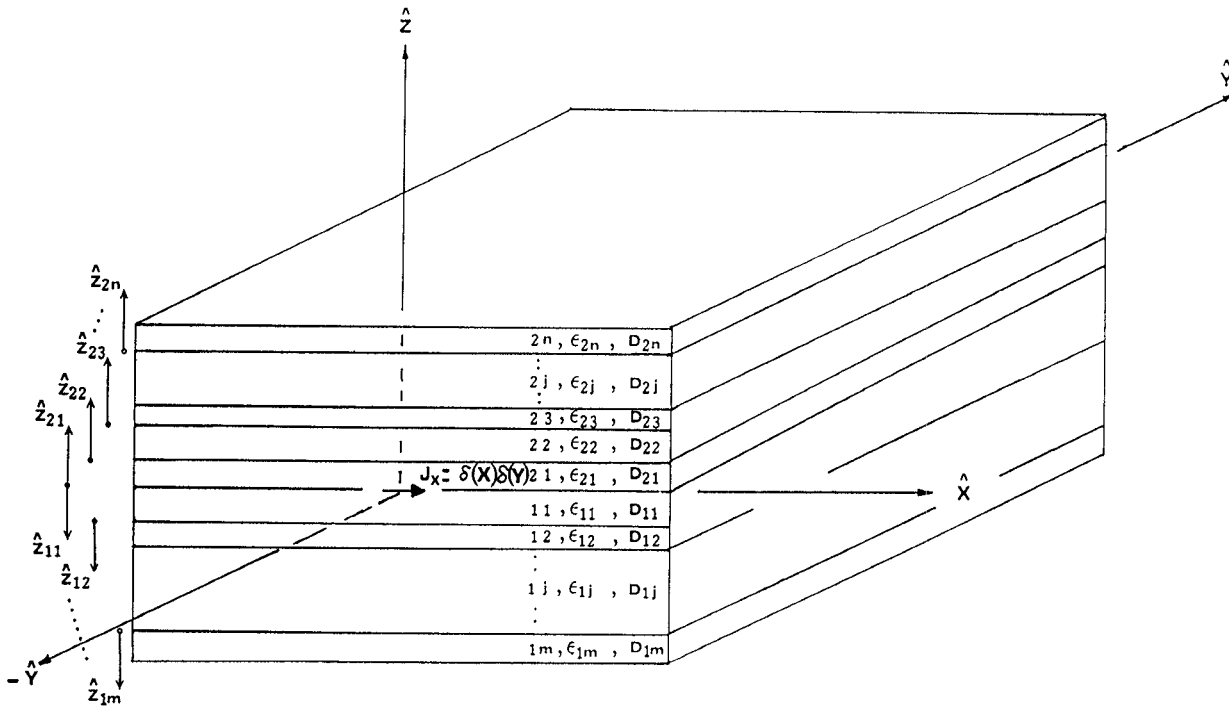


Fig. 1. Geometry of generalized multilayer configuration of dielectric substrates.

dimensions. Critical behaviors are discussed as far as possible in all cases.

In Section II, the Green's function, and the associated iterative algorithm necessary to compute it, are derived. In Section III, the behavior of the Green's function is studied. In Section IV, various transmission-line structures are treated using the derived Green's function, and data are presented.

II. THEORY

A. Decomposition of Field Using Electric and Magnetic Vector Potentials

The field in any region can be completely defined by suitable components of the electric and magnetic vector potentials. In conventional TE or TM (to x , y , or z) decomposition to completely define a field, the choices are (A_x, F_x) , (A_y, F_y) , and (A_z, F_z) , respectively, where the A 's and F 's are components of the vector electric and magnetic potentials. In [1] and [2], the fields have been decomposed using A_x and A_z . But, in fact, any two components of $(A_x, A_y, A_z, F_x, F_y, F_z)$ can completely define a field in any space. The choice is decided, however, by the fact that in some configurations the analysis is greatly simplified by using certain combinations.

In the present analysis, the field is decomposed using (A_z, F_z) , the motivations for which will be justified below. Now, with reference to the coordinate system shown in Fig. 1, the vector potentials are chosen as

$$\bar{A} = A_z(x, y, z)\hat{z} \quad (1)$$

$$\bar{F} = F_z(x, y, z)\hat{z}. \quad (2)$$

For an arbitrary surface-current distribution in the xy plane between the 11 and 21 layers, such that

$$\bar{J}_s(x, y) = J_x(x, y)\hat{x} + J_y(x, y)\hat{y} \quad (3)$$

the solution to A_z , F_z or any component of \bar{E} or \bar{H} can be written using the corresponding Green's function. For example,

$$A_z(x, y, z) = \iint_{\text{source}} \left[G_{A_z J_x}(x, y, z|x_0, y_0) J_x(x_0, y_0) + G_{A_z J_y}(x, y, z|x_0, y_0) J_y(x_0, y_0) \right] dx_0 dy_0. \quad (4)$$

For the Green's function G , the first subscript is the field (\bar{E} or \bar{H}) or potential (A_z or F_z) component and the second subscript is the source component (J_x or J_y). The Green's function for J_x or J_y with the source coordinate at (x_0, y_0) can be obtained by solving Maxwell's equations for the corresponding field or potential component with surface-current density $\bar{J}_s = \delta(x - x_0)\delta(y - y_0)\hat{x}$ or $\bar{J}_s = \delta(x - x_0)\delta(y - y_0)\hat{y}$, respectively.

Now, define a transform pair in two dimensions:

$$\tilde{A}_z(k_x, k_y, z) = \iint_{-\infty}^{\infty} A_z(x, y, z) e^{-jk_x x} e^{-jk_y y} dx dy \quad (5)$$

$$A_z(x, y, z) = \frac{1}{4\pi^2} \int_{-\infty}^{\infty} \int_{-\infty}^{\infty} \tilde{A}_z(k_x, k_y, k_z) e^{jk_x x} e^{jk_y y} dk_x dk_y \quad (6)$$

and similarly for all other components of \bar{E} , \bar{H} , \bar{A} , and \bar{F} . From (5) and (6), and some simple coordinate transformations, it can be shown that in the spectral domain (4) can

be transformed to

$$\begin{aligned} A_z(x, y, z) = & \frac{1}{4\pi^2} \iint_{-\infty}^{\infty} \left[\tilde{G}_{A_z J_x}(k_x, k_y, z|0,0) \tilde{J}_x(k_x, k_y) \right. \\ & + \tilde{G}_{A_z J_x}(k_y, -k_x, z|0,0) \tilde{J}_y(k_x, k_y) \left. \right] \\ & \cdot e^{jk_x x} e^{jk_y y} dk_x dk_y \end{aligned} \quad (7)$$

which means that the Green's function for \tilde{A}_z can be written in vector form as

$$\begin{aligned} \tilde{G}_{A_z J}(k_x, k_y, z) = & \left[\tilde{G}_{A_z J_x}(k_x, k_y, z|0,0) \hat{x} + \tilde{G}_{A_z J_x}(k_y, -k_x, z|0,0) \hat{y} \right]. \end{aligned} \quad (8)$$

Similar equations can be obtained for components of \tilde{E} , \tilde{H} , or \tilde{F}_z .

It can be noted from (7) that the spectral-domain Green's function for the source component J_x only, with the source coordinate at $(0,0)$, can completely define the corresponding dyadic Green's function, and that this can be obtained for different field or potential components by solving Maxwell's equations in the spectral domain for the corresponding field or potential components with

$$\tilde{J}_s = \delta(x)\delta(y)\hat{x}. \quad (9)$$

In the next section, the complete solutions for various field and potential components are derived in the spectral domain with \tilde{J}_s as given in (9). The expressions in spectral form for different field components (\tilde{E}_x , \tilde{E}_y , \tilde{E}_z , \tilde{H}_x , \tilde{H}_y , \tilde{H}_z) and different potential components (\tilde{A}_z , \tilde{F}_z) thus correspond to the Green's functions with source J_x and source coordinate at $(0,0)$.

B. Spectral-Domain Solutions for the Green's Functions

Using the transform equations (5) and (6), and the expression for \tilde{J}_s given in (9), the \tilde{E} and \tilde{H} fields in a source-free region can be written in terms of \tilde{A}_z , \tilde{F}_z as

$$\tilde{E}_x = \frac{k_x}{\omega\epsilon} \cdot \frac{\partial \tilde{A}_z}{\partial z} - jk_y \tilde{F}_z \quad (10)$$

$$\tilde{E}_y = \frac{k_y}{\omega\epsilon} \cdot \frac{\partial \tilde{A}_z}{\partial z} + jk_x \tilde{F}_z \quad (11)$$

$$\tilde{E}_z = \frac{1}{j\omega\epsilon} \left(\frac{\partial^2 \tilde{A}_z}{\partial z^2} + k^2 \tilde{A}_z \right) \quad (12)$$

$$\tilde{H}_x = jk_y \tilde{A}_z + \frac{k_x}{\omega\mu} \cdot \frac{\partial \tilde{F}_z}{\partial z} \quad (13)$$

$$\tilde{H}_y = -jk_x \tilde{A}_z + \frac{k_y}{\omega\mu} \cdot \frac{\partial \tilde{F}_z}{\partial z} \quad (14)$$

$$\tilde{H}_z = \frac{1}{j\omega\mu} \left(\frac{\partial^2 \tilde{F}_z}{\partial z^2} + k^2 \tilde{F}_z \right). \quad (15)$$

The wave equations in the space domain

$$\nabla^2 A_z + k^2 A_z = 0 \quad (16)$$

$$\nabla^2 F_z + k^2 F_z = 0 \quad (17)$$

transform to

$$\frac{\partial^2 \tilde{A}_z}{\partial z^2} + \beta^2 \tilde{A}_z = 0 \quad (18)$$

$$\frac{\partial^2 \tilde{F}_z}{\partial z^2} + \beta^2 \tilde{F}_z = 0 \quad (19)$$

where

$$\beta^2 = k^2 - k_x^2 - k_y^2, \quad k = k_0 \sqrt{\epsilon_r}, \quad \text{Im } \beta < 0. \quad (20)$$

With reference to Figs. 1 and 2, the general solution to (18) and (19) can be written for layer (ij) as

$$\tilde{A}_{z_{ij}} = (e^{-j\beta_{ij} z_{ij}} + \Gamma_{A_{ij}} e^{j\beta_{ij} z_{ij}}) a_{ij}(k_x, k_y) \quad (21)$$

$$\tilde{F}_{z_{ij}} = (e^{-j\beta_{ij} z_{ij}} + \Gamma_{F_{ij}} e^{j\beta_{ij} z_{ij}}) f_{ij}(k_x, k_y) \quad (22)$$

where the Γ_A 's, Γ_F 's, a 's, and f 's are the unknowns to be solved from different boundary conditions at different interfaces. It can be noted here that (21) and (22) are in a form equivalent to the equations for voltage or current waves on a transmission line.

C. The "Standard" Form

For layers 11 and 21, which are at the two sides of the current elements, as shown in Fig. 2, (21) and (22) become

$$\tilde{A}_{z_{11}} = (e^{i\beta_{11} z} + \Gamma_{A_{11}} e^{-j\beta_{11} z}) a_{11} \quad (23)$$

$$\tilde{A}_{z_{21}} = (e^{-j\beta_{21} z} + \Gamma_{F_{21}} e^{j\beta_{21} z}) a_{21} \quad (24)$$

$$\tilde{F}_{z_{11}} = (e^{j\beta_{11} z} + \Gamma_{A_{11}} e^{-j\beta_{11} z}) a_{21} \quad (25)$$

$$\tilde{F}_{z_{21}} = (e^{-j\beta_{21} z} + \Gamma_{F_{21}} e^{j\beta_{21} z}) f_{21}. \quad (26)$$

In these expressions, the Γ 's are unknowns to be determined by solving the boundary conditions at other interfaces, and hence are functions of the parameters of other layers. These are considered known in this section. So, we have four unknowns, a_{11} , a_{21} , f_{11} , f_{21} , which can be solved as a function of $\Gamma_{A_{11}}$, $\Gamma_{A_{21}}$, $\Gamma_{F_{11}}$, $\Gamma_{F_{21}}$ by solving four boundary conditions in the spectral domain: (i) \tilde{E}_x , (ii) \tilde{E}_y , (iii) \tilde{H}_x are continuous across the boundary between layers 11 and 21, and (iv)

$$\tilde{H}_{y_{21}} - \tilde{H}_{y_{11}}|_{z=0} = 1. \quad (27)$$

These boundary conditions, along with the spectral-domain field expressions (10)–(15) result in a set of simultaneous equations to be solved for a_{21} , f_{21} , a_{11} , and f_{11} . The results are

$$f_{21} = \frac{k_y \omega \mu_0 (1 + \Gamma_{F_{11}})}{T_e (k_x^2 + k_y^2)} \quad (28)$$

$$a_{21} = \frac{k_x (1 - \Gamma_{A_{11}}) \beta_{11} / \epsilon_{11}}{T_m (k_x^2 + k_y^2)} \quad (29)$$

$$f_{11} = \frac{k_y \omega \mu_0 (1 + \Gamma_{F_{21}})}{T_e (k_x^2 + k_y^2)} \quad (30)$$

$$a_{11} = \frac{-k_x (1 - \Gamma_{A_{21}}) \beta_{21} / \epsilon_{21}}{T_m (k_x^2 + k_y^2)} \quad (31)$$

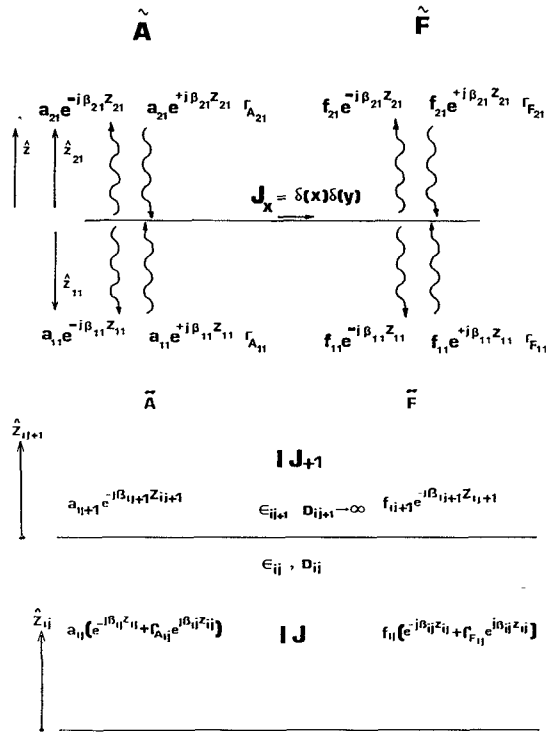


Fig. 2. Electric current element (top) at the interface of two layers, 11 and 21 (the "standard" problem) and the boundary (bottom) between two generalized layers, (I, J) and $(I, J+1)$, not containing the current element between them, with the second layer extending to infinity.

where

$$T_m = j[\beta_{11}/\epsilon_{11}(1 + \Gamma_{A_{21}})(1 - \Gamma_{A_{11}}) + \beta_{21}/\epsilon_{21}(1 + \Gamma_{A_{11}})(1 - \Gamma_{A_{21}})] \quad (32)$$

$$T_e = j[\beta_{11}(1 - \Gamma_{F_{11}})(1 + \Gamma_{F_{21}}) + \beta_{21}(1 - \Gamma_{F_{21}})(1 + \Gamma_{F_{11}})]. \quad (33)$$

Equations (28)–(33) along with (23)–(26) define the solutions for \tilde{A}_z and \tilde{F}_z in the 11 and 21 layers in terms of $\Gamma_{A_{11}}, \Gamma_{A_{21}}, \Gamma_{F_{11}}, \Gamma_{F_{21}}$, and are referred to as the standard solutions for \tilde{A}_z and \tilde{F}_z , respectively. By using (10)–(15), and the standard solutions for \tilde{A}_z and \tilde{F}_z , the corresponding standard solutions for \bar{E} and \bar{H} can be obtained. These standard expressions are applicable to any multilayer structure having the standard source structure of Fig. 2. The effect of other layers is taken into account via the Γ 's. These Γ 's are functions of the parameters of other layers (thickness, dielectric constant) and can be obtained by solving Maxwell's equations in the other layers with suitable boundary conditions (continuity of all fields) between any two adjacent layers.

D. Boundary Conditions at Other Interfaces

The boundary conditions at other interfaces can be solved by using the transformed field equations (10)–(15) and continuity of $\tilde{E}_x, \tilde{E}_y, \tilde{H}_x, \tilde{H}_y$ across the boundaries. It can be noted here that with the choice of electric and magnetic vector potentials, the boundary conditions can be solved separately for \tilde{A}_z and \tilde{F}_z . With other choices of \tilde{A}

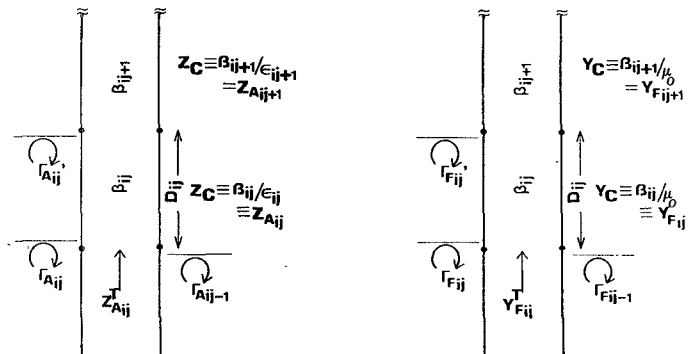


Fig. 3. The transmission line models for \tilde{A}_z and \tilde{F}_z showing the equivalences between different transmission-line and field parameters.

and \tilde{F} , this would not have been possible, since coupled equations would result.

The Γ 's of the field expressions are found to be equivalent to reflection coefficients for a transmission line terminated by another infinite transmission line of different characteristic impedance, as shown in Fig. 3. For the magnetic potential, the equivalent transmission-line impedance is equal to (β/ϵ) , which is the same as the TM wave impedance, while for the electric potential the equivalent transmission-line admittance is equal to (β/μ) , which is same as the TE wave admittance. Also, the reflection coefficient for \tilde{A}_z is equivalent to the reflection coefficient of a current wave in a transmission line, while the reflection coefficient for \tilde{F}_z is equivalent to that of a voltage wave in a transmission line.

These equivalences can be written in terms of the following equations:

$$\Gamma_{A_{ij}} = \frac{(Z_{A_{ij}} - Z_{A_{ij+1}})}{(Z_{A_{ij}} + Z_{A_{ij+1}})} = \frac{(\beta_{ij}/\epsilon_{ij} - \beta_{ij+1}/\epsilon_{ij+1})}{(\beta_{ij}/\epsilon_{ij} + \beta_{ij+1}/\epsilon_{ij+1})} \quad (34)$$

$$\Gamma'_{F_{ij}} = \frac{(Y_{F_{ij}} - Y_{F_{ij+1}})}{(Y_{F_{ij}} + Y_{F_{ij+1}})} = \frac{(\beta_{ij} - \beta_{ij+1})}{(\beta_{ij} + \beta_{ij+1})} \quad (35)$$

where

$$Z_{A_{ij}} = \beta_{ij}/\epsilon_{ij} \quad Y_{F_{ij}} = \beta_{ij}/\mu_{ij} = \beta_{ij}/\mu_0. \quad (36)$$

For the case when the second layer is a perfect electric conductor (pec), we have

$$\Gamma'_{A_{pec}} = 1 \quad Z_{A_{pec}} = 0 \quad (37)$$

$$\Gamma'_{F_{pec}} = -1 \quad Y_{F_{pec}} = \infty. \quad (38)$$

The above formulation was for the case where the second medium is of infinite extent. But if it is finite, and is covered with another layer and so on, we can generalize the expressions for $\Gamma_{A_{ij}}, \Gamma_{F_{ij}}$ using transmission-line equations. The boundary conditions can be solved again for all the interfaces, and the general results given below can be derived. The expressions for Γ 's are given in terms of iterative formulas as

$$\Gamma_{A_{ij}} = \Gamma'_{A_{ij}} e^{-2j\beta_{ij}D_{ij}} = e^{-2j\beta_{ij}D_{ij}} \frac{(Z_{A_{ij}} - Z_{A_{ij+1}})}{(Z_{A_{ij}} + Z_{A_{ij+1}})} \quad (39)$$

and similarly,

$$\Gamma_{F_{ij}} = e^{-j\beta_{ij}D_{ij}} \frac{(Y_{F_{ij}} - Y_{F_{ij+1}}^T)}{(Y_{F_{ij}} + Y_{F_{ij+1}}^T)} \quad (40)$$

where

$$Z_{A_{ij+1}}^T = \frac{(1 - \Gamma_{A_{ij+1}})}{(1 + \Gamma_{A_{ij+1}})} Z_{A_{ij+1}} \quad (41)$$

$$Y_{F_{ij+1}}^T = \frac{(1 + \Gamma_{F_{ij+1}})}{(1 - \Gamma_{F_{ij+1}})} Y_{F_{ij+1}}. \quad (42)$$

With the above iterative expressions $\Gamma_{A_{11}}$, $\Gamma_{A_{21}}$, $\Gamma_{F_{11}}$, $\Gamma_{F_{21}}$ may be found in terms of k_x , k_y and $\epsilon_{r_{ij}}$, D_{ij} for all layers. Thus, the Green's functions for \tilde{A}_z and \tilde{F}_z are obtained by the use of (28)–(33) and the expressions for the Γ 's. The Green's functions for \bar{E} and \bar{H} are then derived using (10)–(15).

For more than one layer, if the final form of the Green's function is written in terms of the individual ϵ 's and D 's, it becomes extremely complex. So, it is advisable to use the iterative formula in the form given in (39)–(42) as a part of the numerical computation of the Green's function. In a way, then, the Green's function is obtained numerically rather than in closed form. For some specific geometries, the Green's functions for \bar{E} and \bar{H} can be obtained without undue complexity.

The Green's functions obtained so far are valid for layers 11 and 21. To be complete, we must find the Green's functions in the other layers as well, which can be done by using (10)–(15) and (21)–(22), where the f 's, a 's, and Γ 's are obtained from a transmission-line analogy. An iterative algorithm to compute a_{ij+1} from a_{ij} is

$$\begin{aligned} a_{ij+1} &= a_{ij} \frac{(1 + \Gamma'_{A_{ij}})}{(1 + \Gamma_{A_{ij+1}})} e^{-j\beta_{ij}D_{ij}} \\ &= 2e^{-j\beta_{ij}D_{ij}} a_{ij} Z_{A_{ij}} \\ &\quad \left/ \left[(1 + \Gamma_{A_{ij+1}}) \left(Z_{A_{ij}} + \frac{1 - \Gamma_{A_{ij+1}}}{1 + \Gamma_{A_{ij+1}}} Z_{A_{ij+1}} \right) \right] \right. \end{aligned} \quad (43)$$

and similarly,

$$f_{ij+1} = 2e^{-j\beta_{ij}D_{ij}} f_{ij} Y_{F_{ij}} \left/ \left[(1 + \Gamma_{F_{ij+1}}) \left(Y_{F_{ij}} + \frac{1 - \Gamma_{F_{ij+1}}}{1 + \Gamma_{F_{ij+1}}} Y_{F_{ij+1}} \right) \right] \right. \quad (44)$$

III. BEHAVIOR OF THE GREEN'S FUNCTION

A. Asymptotic Form

The Green's function which has been derived is computationally complex, and the complexity increases with the number of layers. But because of the form in which the Green's function is derived, there is the possibility of asymptotically simplifying it into a Green's function for a simpler equivalent structure. The $\alpha = \sqrt{k_x^2 + k_y^2}$ limit be-

yond which the original Green's function converges to the equivalent asymptotic form is also given. Hence, beyond this asymptotic limit, all multilayer structures can be treated as a simple two-layer problem.

For large $\alpha > k_0 \sqrt{\epsilon_{r_{\max}}}$, where $\epsilon_{r_{\max}} = \max(\epsilon_{r_{ij}})$,

$$\beta_{ij} = -j\sqrt{\alpha^2 - k^2} = -j\alpha \quad \text{for all } i, j. \quad (45)$$

From (34)–(36), it can be shown that the Z_A 's and Y_A 's are real, which implies that $|\Gamma'_{A_{ij}}| < 1$ and $|\Gamma_{A_{ij}}| < e^{-2\alpha D_{ij}}$. Hence, for $\alpha > \alpha_{\text{th}}$, such that $e^{-2\alpha_{\text{th}} D_{ij}}$ is less than some preassigned arbitrary small value τ ,

$$|\Gamma_{A_{ij}}| \approx 0 \quad (46)$$

and so all the layers above the (ij) layer are equivalent to one infinite extension of the substrate at the ij layer (for an infinite layer, the Γ_A 's and Γ_F 's are zero) in the asymptotic limit. Hence, in the asymptotic limit, all multilayer structures are equivalent to the structure containing the immediate two layers, extended to infinity, on each side of the current element. The reason for this is that large values of α account for the reactive field of the source, which is a localized effect. As an example, Fig. 4 shows the asymptotic behavior of the Green's function ($|\tilde{G}|$) for various multilayer configurations having the same 11 and 21 (standard) layers. All cases converge to curve no. 7, the results for two semi-infinite layers.

With the above argument, the asymptotic expressions for the Green's functions of the components of \bar{E} , \bar{H} , A_z , and F_z can be obtained from the corresponding standard expressions by replacing the Γ 's with 0's. Thus, in the asymptotic limit

$$f_{21} = f_{11} = \frac{k_y \omega \mu}{T_e \alpha^2} \quad (47)$$

$$a_{11} = \frac{-k_x \beta_{21}}{\epsilon_{21} T_m \alpha^2} \quad (48)$$

$$a_{21} = \frac{k_x \beta_{11}}{\epsilon_{11} T_m \alpha^2} \quad (49)$$

where

$$T_m = j(\beta_{11}/\epsilon_{11} + \beta_{21}/\epsilon_{21}) \quad (50)$$

$$T_e = j(\beta_{11} + \beta_{21}). \quad (51)$$

The worst-case asymptotic limit occurs for the greater of α_1 or α_2 such that

$$e^{-2\alpha_1 D_{11}} < \tau \text{ and } e^{-2\alpha_2 D_{21}} < \tau \quad (52)$$

where τ is a preassigned small value.

With similar arguments, the following conclusions can be drawn regarding the behavior of the Green's functions for multilayer structures.

1) The Green's function for a field point different from the plane of the current element exciting it is exponentially convergent with α , which implies that the computation of mutual coupling between two current patches on different planes converges much faster than that of self-reaction or

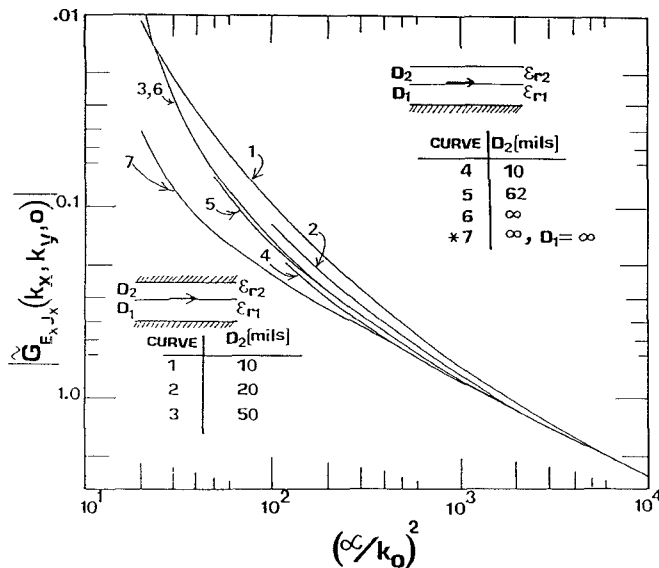


Fig. 4. Convergence of $\tilde{G}_{E_x, J_x}(k_x, k_y, 0, 0, 0)$ with $\alpha = \sqrt{2} k_x = \sqrt{2} k_y$ to a single asymptotic form (curve no. 7) having $D_{21} = D_2 = \infty$ and $D_{11} = D_1 = \infty$ for a number of multilayer configurations of the same standard structure ($\epsilon_{r21} = \epsilon_{r2} = 2.2$, $\epsilon_{r11} = \epsilon_{r1} = 10.2$, $D_{11} = D_1 = 50$ mil) at 3 GHz.

mutual coupling between current patches in the same plane.

2) The worst-case asymptotic limit given by (52), beyond which the Green's function converges to the proposed asymptotic form of (47)–(51), depends on the thicknesses of the layers adjacent to the current element. This effect is shown in Fig. 4, which shows that convergence to the asymptotic limit is faster for thicker layers.

3) The Green's function for a structure with a ground plane ($|\Gamma| = 1$) converges slowly in comparison to a similar structure without a ground plane; e.g., the Green's function for a stripline structure with two dielectrics converges more slowly than the Green's function for a covered microstrip structure with the same two dielectrics. This effect is shown in Fig. 4 by curve no. 1 (a stripline-type geometry), and curve no. 4 (a covered microstrip-line-type geometry).

4) The convergence of f_{21} and f_{11} is of the order of $1/\alpha^2$, whereas the convergence of a_{21} and a_{11} is $1/\alpha$. Hence, from (10)–(15), it can be concluded that the Green's function for \tilde{E} is dominated in the asymptotic limit by the contribution from \tilde{A}_z , being of the order of α^1 , whereas the contribution from \tilde{F}_z is of the order of α^{-1} . Thus, in the asymptotic limit, the spectral-domain solution for \tilde{E} can be treated as TM to z .

5) The significant difference between the Green's functions for different multilayer structures with the same standard substructure lies in the smaller values of α , but for higher values of α (typically greater than $20k_0$), all these structures can be treated as equivalent to the standard structure, with the substrates on both sides of the current element extending to infinity. Then, the techniques for this simple two-layer structure can be applied without any problem [3], [4].

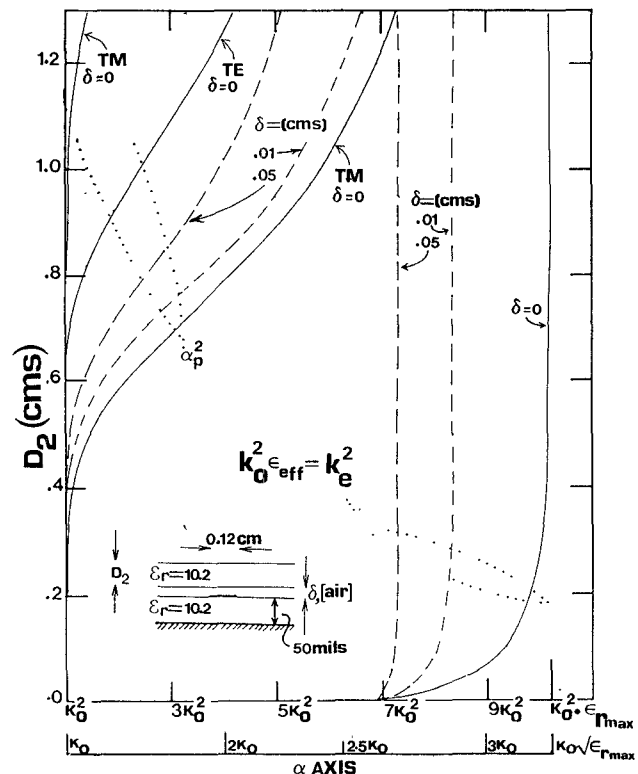


Fig. 5. The locus of all the TE, TM surface wave poles (α_p) at 3 GHz along the α axis, in the range $k_0 \leq \alpha_p \leq k_0 \sqrt{\epsilon_{r_{\max}}}$ and with different cover heights ($D_{21} = D_2$), for a covered microstrip line and the corresponding locus of the effective dielectric constants. The locus of the highest surface wave poles for the same covered microstripline with an air gap (δ) between the two dielectric layers and the corresponding locus of ϵ_{eff} for the same w are also shown.

B. TM and TE Poles of the Green's Function

An important point to be considered for the spectral-domain integration of the Green's function is the treatment of the surface wave poles. The poles of a Green's function component can be found from the zeros of the T_e and T_m expressions of (34) and (35). Sometimes, one pole of a Green's function due to a zero of T_e or T_m , which appears in the denominator, may be removable due to a zero of equal order in the numerator.

The TE and TM poles of the Green's function due to zeros of the T_e and T_m expressions, respectively, can be interpreted as possible excitation of TE or TM surface wave modes (in the case of microstrip-line structures) or possible excitation of TE or TM waveguide modes (in the case of stripline structures). Whether these modes are actually excited or not in a given problem remains to be determined.

It has been found that all the poles of any Green's function component lie between k_0 and $k_0 \sqrt{\epsilon_{r_{\max}}}$. In this interval, the T_e , T_m expressions can be searched for zeros by using an exhaustive search technique. Using the Newton-Raphson method, the poles of the Green's function for different multilayer structures can be determined, and some results are given in Fig. 5 for covered microstrip structures with variable air gaps.

IV. APPLICATION TO MULTILAYER PLANAR TRANSMISSION LINES

With reference to Fig. 1, for a multilayer microstrip or strip transmission line in the \hat{x} direction with the conductor running between layers 11 and 21 and having width w in the \hat{y} direction, the expression for the surface-current density on the conductor can be written as

$$\bar{J}_s(x, y) = e^{-jk_e x} f(y) \hat{x} \quad (53)$$

where $k_e (= k_0 \sqrt{\epsilon_{\text{eff}}})$ is the effective propagation constant and $f(y)$ is the transverse variation of current density on the conducting line. Using (53) and an equation similar to (9) with $\tilde{G}_{E_x J_x}$ instead of $\tilde{G}_{A_x J_x}$ gives

$$\begin{aligned} & \int_{-w/2}^{w/2} J_x(x, y) E_x(x, y, 0) dy \\ &= \frac{1}{4\pi^2} \int_{-\infty}^{\infty} \tilde{G}_{E_x J_x}(-k_e, k_y, 0 | 0, 0) F(k_y)^2 dk_y \quad (54) \end{aligned}$$

where

$$F(k_y) = \int_{-w/2}^{w/2} f(y) e^{-jk_y y} dy = \frac{\sin(k_y w/2)}{k_y w/2} \quad (55)$$

and $\tilde{G}_{E_x J_x}$ is obtained from the expressions of $\tilde{G}_{A_x J_x}$ and $\tilde{G}_{F_x J_x}$ and (10).

The left-hand side of (54) can be equated to zero [7]; hence, ϵ_{eff} can be found by solving the following integral equation:

$$\int_{-\infty}^{\infty} \tilde{G}_{E_x J_x}(-k_e, k_y, 0 | 0, 0) F(k_y)^2 dk_y = 0. \quad (56)$$

This integral equation was solved using the interval-halving method. In the integration, the poles of the integrand were carefully taken into account. It was observed, however, that the effective dielectric constant obtained by solving (56) was always greater than $(\alpha_{p\max}/k_0)^2$, where $\alpha_{p\max}$ is the highest pole of the Green's function of the microstrip-line structure, confirming the fact that there is no excitation of surface wave power in an infinite microstrip line [7]. An example of this effect is shown in Fig. 5 for covered microstrip line with a variable air gap. But for a stripline structure, the effective dielectric constant may be greater than, equal to, or less than the corresponding $(\alpha_{p\max}/k_0)^2$, leading to probable excitation of some waveguide modes.

The characteristic impedance was found using the following equation:

$$\begin{aligned} Z_c &= -\frac{1}{4\pi^2} \left[\int_{\text{gp}}^{z=0} \int_{-\infty}^{\infty} \tilde{G}_{E_x J_x}(-k_e, k_y, z) F(k_y)^2 dk_y dz \right] \\ &\quad \left/ \left[\int_{-w/2}^{w/2} f(y) dy \right] \right. \\ &= \left[\int_{\text{gp}}^{z=0} \int_{-w/2}^{w/2} -E_z(x, y, z) J_x^*(x, y) dy dz \right] \\ &\quad \left/ \left[\int_{-w/2}^{w/2} f(y) dy \right] \right. \\ &= \frac{V_{\text{av}}}{I} \quad (57) \end{aligned}$$

on the conductor with respect to the ground plane (gp).

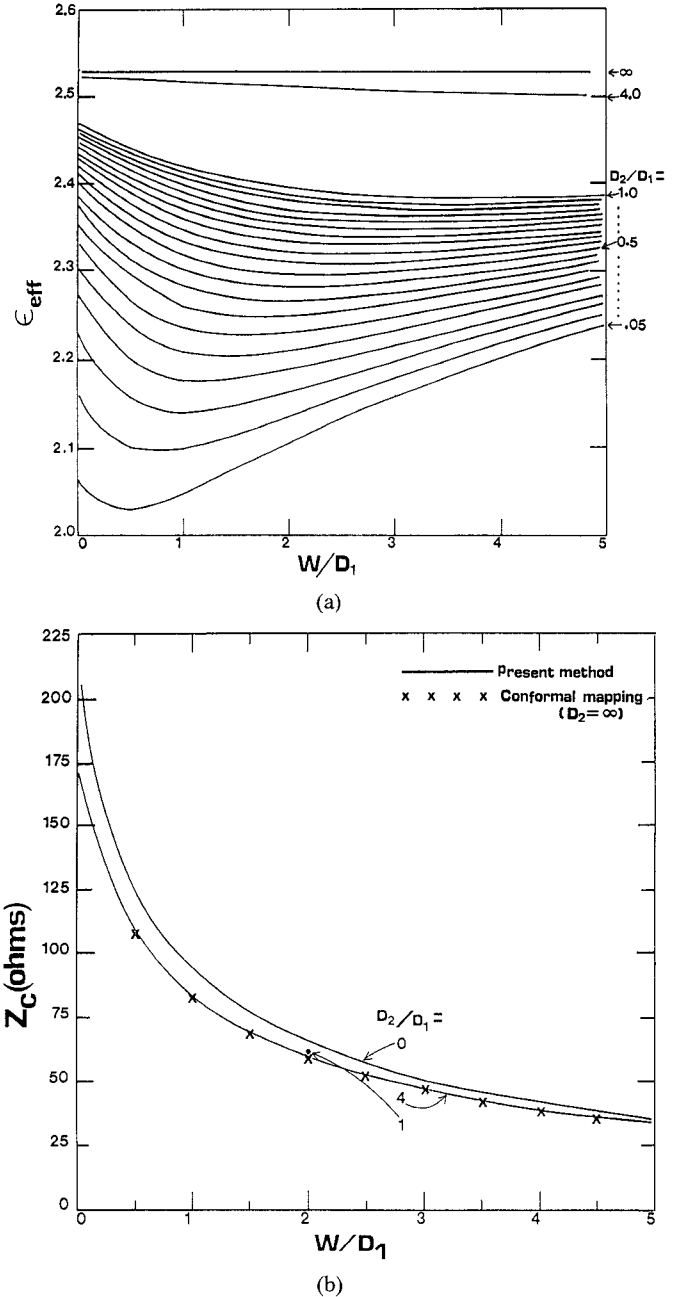
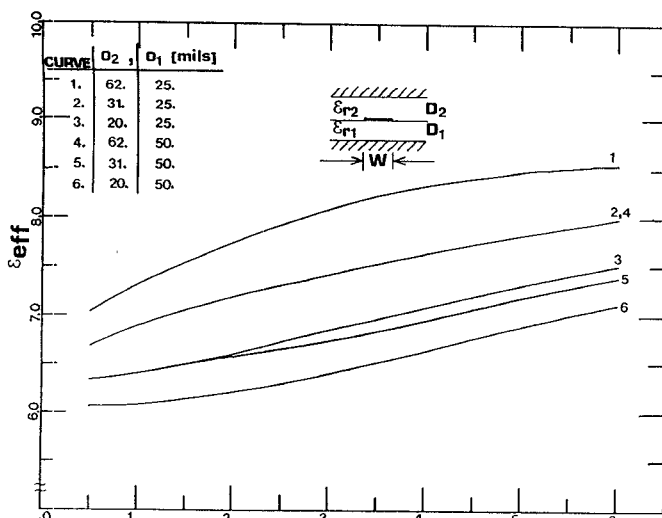


Fig. 6. (a) ϵ_{eff} of a covered microstrip line as a function of w/D_1 , with D_2/D_1 as a parameter. (b) Characteristic impedance (Z_c) of the above covered microstrip line with $\epsilon_{r2} = 2.53$, $\epsilon_{r1} = 2.53$ as a function of w for various cover thicknesses D_2/D_1 .

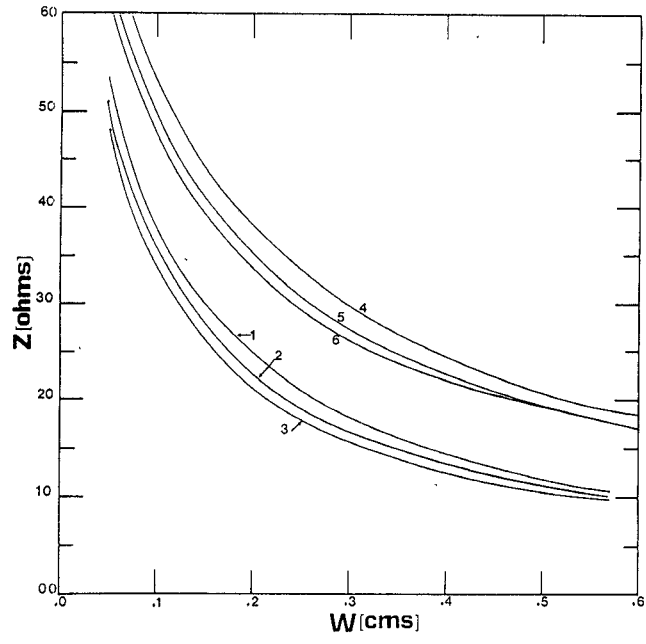
For convenience, so far as equivalence to the generalized structure of Fig. 1 is concerned, in this section, ϵ_{r1} , ϵ_{r2} , D_1 , and D_2 are referred to respectively, as ϵ_{r11} , ϵ_{r21} , D_{11} , and D_{21} for microstrip and strip lines without an air gap and as ϵ_{r11} , ϵ_{r22} , D_{11} , and D_{22} for microstrip and strip lines with an air gap (δ); the air gap is the 21 layer, $\epsilon_{r21} = 1.0$, and $\delta = D_{21}$.

A. Microstrip Line with a Dielectric Cover

The analysis was applied to the case where the dielectric constant of the cover substrate was the same as that of the original microstrip line. The effective dielectric constant (ϵ_{eff}) and characteristic impedance (Z_c) are parts (a) and (b) shown in Fig. 6 for a covered microstrip line with



(a)

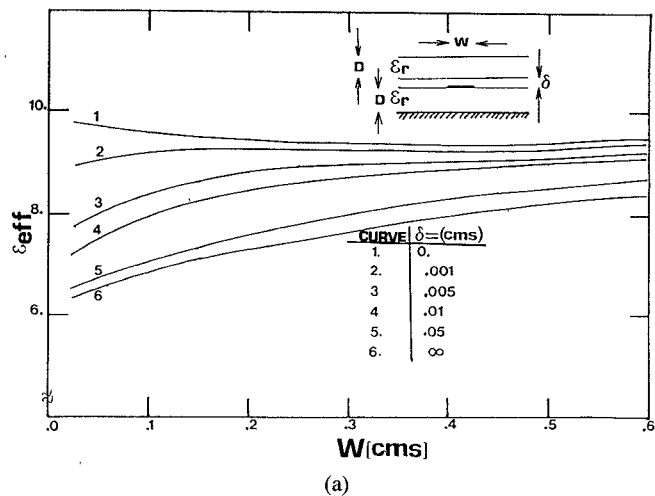


(b)

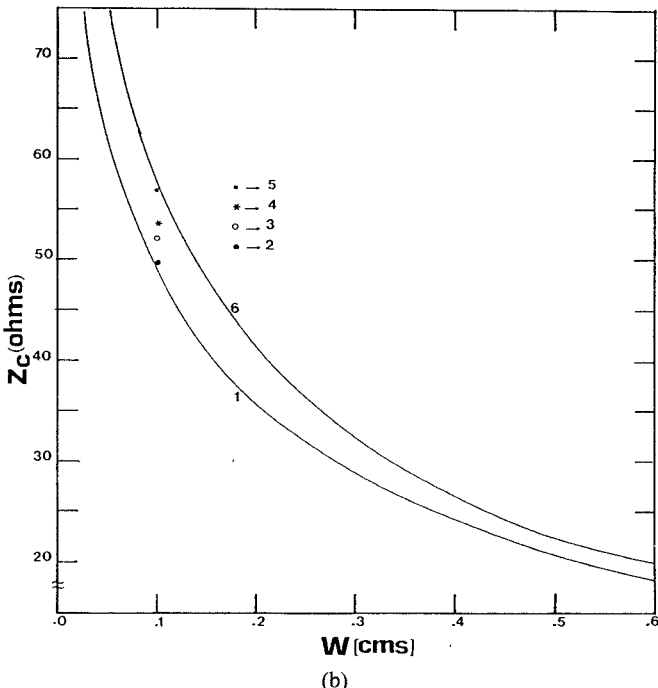
Fig. 7. (a) ϵ_{eff} and (b) Z_c as a function of w for a stripline with $\epsilon_{r2} = 2.2$, $\epsilon_{r1} = 10.2$ at 3 GHz for different combinations of D_2 and D_1 .

$\epsilon_r = 2.53$ as a function of w/D_1 , and D_2/D_1 as a parameter. The characteristic impedance Z_c is not affected significantly by the cover substrate, but the effective dielectric constant changes drastically with the cover height. For smaller values of line width w , the effective dielectric constant of this type of covered microstrip line is very sensitive to even very thin covers. Unlike the uncovered microstrip line, the effective dielectric constant for a covered microstrip line decreases with an increase in the width (w) of the conductor for smaller values of w . This trend is more prominent over a larger region of w for thicker cover substrates.

For a large value of cover height (D_2), as shown in Fig. 6(a), the covered microstrip line behaves as a TEM line with ϵ_{eff} equal to ϵ_r . In Fig. 6(b), the characteristic impedance for $D_2/D_1 = 4.0$ is compared with $Z_{c(\text{air})}/\sqrt{\epsilon_r}$, where



(a)



(b)

Fig. 8. (a) ϵ_{eff} and (b) Z_c as a function of w for a covered microstrip line with $\epsilon_{r2} = \epsilon_{r1} = \epsilon_r = 10.2$, $D_2 = D_1 = D = 50$ mil and an air gap (δ) at 3 GHz.

$Z_{c(\text{air})}$ is the characteristic impedance of the equivalent air microstrip line, obtained exactly using a conformal mapping technique [11].

B. Striplines with Two Different Dielectric Substrates

The Green's function is now applied to striplines with two different dielectric substrates on the two sides of the conductor. The effective dielectric constant of this type of stripline is shown in Fig. 7(a), and does not vary if the ratio of D_2 to D_1 is unchanged. The corresponding characteristic impedances, shown in Fig. 7(b), depend on the individual thicknesses of the two substrates (D_1 and D_2) rather than on their ratio. As expected, the trend of the effective dielectric constant decreases with a decrease in the thickness of the smaller dielectric constant substrate, and increases with a decrease in the thickness of the larger dielectric constant substrate. This is because a greater

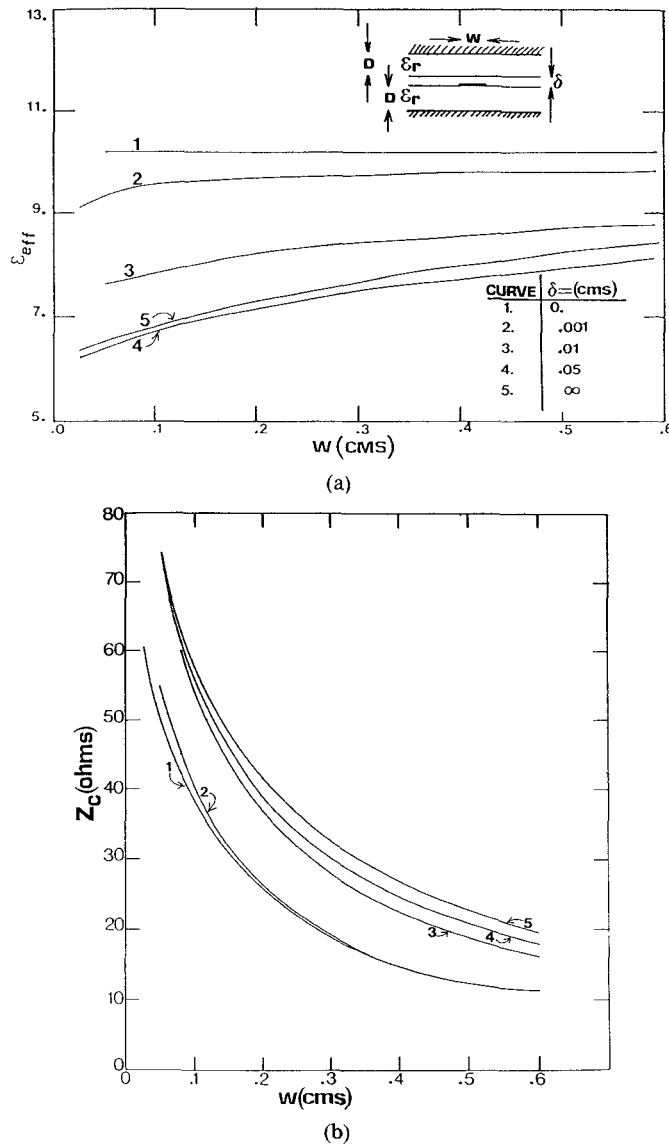


Fig. 9. (a) ϵ_{eff} and (b) Z_c as a function of w for a stripline with $\epsilon_{r2} = \epsilon_{r1} = 10.2$, $D_2 = D_1 = D = 50$ mil and an air gap (δ) at 3 GHz.

percentage of the total field goes into a substrate when the thickness of that substrate decreases.

C. Effect of Air Gaps Introduced Between Two Layers of Covered Microstrip Line or Stripline

The air-gap introduced while fabricating a covered microstrip line or a stripline, by overlapping one substrate on another, is found to have a very significant effect on the effective dielectric constant of the transmission line, as shown in Fig. 8(a) (microstrip) and Fig. 9(a) (stripline). It is particularly drastic for smaller values of the width of the transmission line. The corresponding characteristic impedances, shown in Fig. 8(b) and Fig. 9(b), respectively, are found to be relatively insensitive to the air gap. For example, the ϵ_{eff} can change from a high of 9.6 to a low of 8.0 for a covered microstrip line with $\epsilon_{r2} = \epsilon_{r1} = 10.2$ and $w = 0.1$ cm (50- Ω line) if an air gap of 0.01 cm is introduced; the corresponding increase in characteristic impedance is from 50 Ω to 53 Ω .

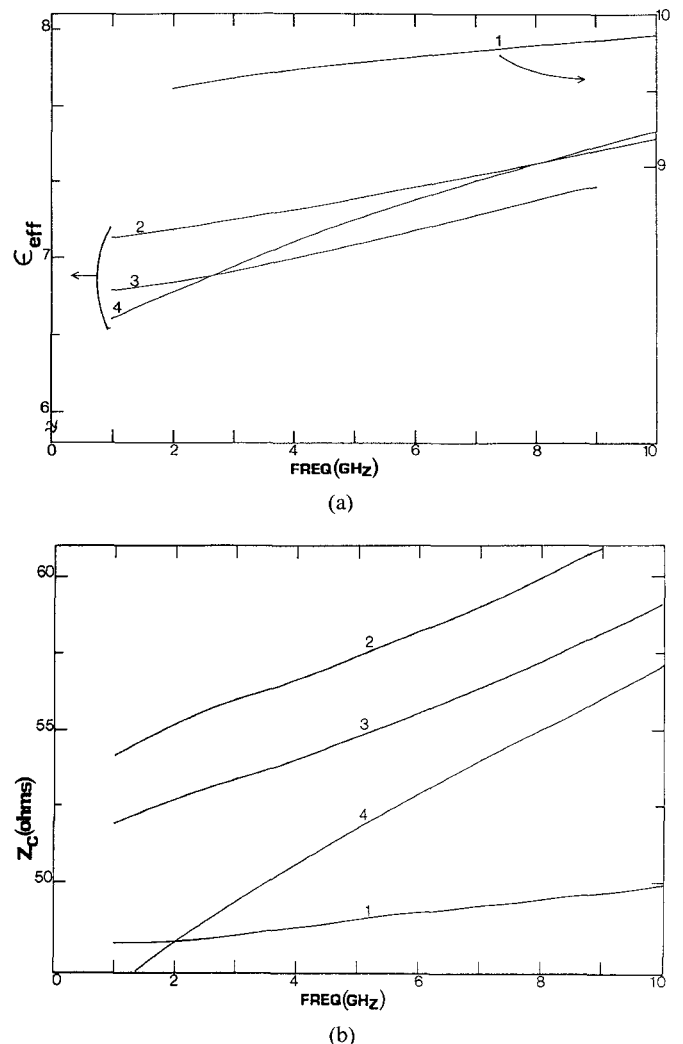


Fig. 10. (a) ϵ_{eff} and (b) Z_c showing the dispersion characteristics of (1) a covered microstrip line with $\epsilon_{r2} = \epsilon_{r1} = 10.2$, $w = 0.1$ cm, and $D_2 = D_1 = 50$ mil; (2) a covered microstrip line with $\epsilon_{r1} = 10.2$, $\epsilon_{r2} = 2.2$, $D_1 = 50$ mil, $D_2 = 50$ mil, and $w = 0.1$ cm; (3) a microstrip line with $\epsilon_{r1} = 10.2$, $D = 50$ mil, and $w = 0.12$ cm; and (4) a stripline with $\epsilon_{r1} = 10.2$, $\epsilon_{r2} = 2.2$, $D_1 = 50$ mil, $D_2 = 62$ mil, and $w = 0.12$ cm.

D. Comparison of Dispersions for Different Transmission Lines

Because the analysis uses the full-wave Green's function, it can treat dispersion in multilayer transmission lines exactly. The relative degrees of dispersion in different configurations of planar transmission lines are compared in parts (a) and (b) of Fig. 10 for frequencies up to 10 GHz. A stripline with two different dielectrics is found to be relatively more dispersive than a covered microstrip line. The dispersion is more if the two dielectric constants are markedly different, as expected. A covered microstrip line with a cover of the same dielectric constant is less dispersive than the corresponding microstrip line without a cover.

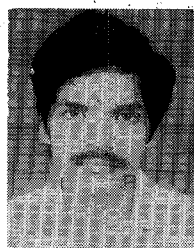
V. CONCLUSIONS

A computer program was developed to compute the generalized Green's function using the exact as well as the asymptotic forms derived in this paper. The program was

used to find the effective dielectric constant ϵ_{eff} and characteristic impedance Z_c of any arbitrary multilayer microstrip or strip transmission line. TE and TM poles were accurately determined and taken into account, and the validity of using the asymptotic form was verified. It is thus concluded that this generalized Green's function can be conveniently used for numerical solutions of various multilayer transmission line and antenna structures.

REFERENCES

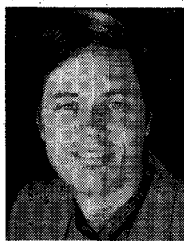
- [1] D. M. Pozar, "Input impedance and mutual coupling of rectangular microstrip antennas," *IEEE Trans. Antennas Propagat.*, vol. AP-30, pp. 1191-1196, Nov. 1982.
- [2] M. C. Bailey and M. D. Deshpande, "Integral equation formulation of microstrip antennas," *IEEE Trans. Antennas Propagat.*, vol. AP-30, pp. 651-656, July 1982.
- [3] M. Kominami *et al.*, "Dipole and slot elements and arrays on semi-infinite substrates," *IEEE Trans. Antennas Propagat.*, vol. AP-33, pp. 600-607, June 1985.
- [4] D. M. Pozar, "Improved computational efficiency for the moment method solution of printed dipoles and patches," *J. Electromagn. Soc.*, vol. 3, nos. 3-4, pp. 299-309, July-Dec. 1983.
- [5] D. M. Pozar, "Considerations for millimeter wave printed antennas," *IEEE Trans. Antennas Propagat.*, vol. AP-31, pp. 740-747, Sept. 1983.
- [6] D. M. Pozar, "General relations for a phased array of printed antennas derived from infinite current sheets," *IEEE Trans. Antennas Propagat.*, vol. AP-33, pp. 498-504, May 1985.
- [7] R. W. Jackson and D. M. Pozar, "Full-wave analysis of microstrip open-end and gap discontinuities," *IEEE Trans. Microwave Theory Tech.*, vol. MTT-33, pp. 1036-1042, Oct. 1985.
- [8] T. Itoh, "Spectral domain immittance approach for dispersion characteristics of generalized printed transmission lines," *IEEE Trans. Microwave Theory Tech.*, vol. MTT-28, pp. 733-736, July 1980.
- [9] A. Farrar and A. T. Adams, "Multilayer microstrip transmission lines," *IEEE Trans. Microwave Theory Tech.*, vol. MTT-22, pp. 889-891, Oct. 1974.
- [10] J. B. Davies and D. Mirshekar-Syahkal, "Spectral domain solution of arbitrary coplanar transmission line with multilayer substrates," *IEEE Trans. Microwave Theory Tech.*, vol. MTT-25, pp. 143-146, Feb. 1977.
- [11] M. V. Schneider, "Microstriplines for microwave integrated circuits," *Bell Syst. Tech. J.*, p. 1421, May-June 1969.
- [12] S. S. Bedair and M. I. Sobhy, "Tolerance analysis of shielded microstriplines," *IEEE Trans. Microwave Theory Tech.*, vol. MTT-32, pp. 544-547, May 1984.



Nirod K. Das was born in Puri, Orissa state, India, on February 27, 1963. He received the B. Tech. degree (with honors) in electronics and electrical communication engineering from the Indian Institute of Technology (IIT), Kharagpur, India, in 1985. He joined, as a graduate research assistant, the Department of Electrical and Computer Engineering at the University of Massachusetts, Amherst, in 1985 and since then has been working for the M.S. and Ph.D. degrees.

His research interests are in the areas of printed antennas, in particular, the analytical and experimental study of multiple-layer integrated-circuit antenna structures for phased-array applications.

✖



David M. Pozar (S'74-M'80) was born in Pittsburgh, PA, on January 25, 1952. He received the B.S. degree in 1975 and the M.S. degree in 1976, both in electrical engineering, from the University of Akron. He received the Ph.D. degree in electrical engineering from Ohio State University in 1980.

During the course of his undergraduate degree, he spent one year as an Engineering Assistant at the National Security Agency, Fort Meade, MD. He was a Graduate Research Assistant in the ElectroScience Lab at Ohio State University while pursuing the Ph.D. degree, and became a Research Assistant upon completion of the Ph.D. degree. He joined the faculty at the University of Massachusetts in 1980, and in 1985 he became an Associate Professor of Electrical and Computer Engineering.

Dr. Pozar belongs to the Antennas and Propagation Society and the Microwave Theory and Techniques Society of the Institute of Electrical and Electronics Engineers (IEEE). He is also an Associate Member of the International Union of Radio Science (URSI), Commission B. He has served as an Associate Editor of the *IEEE TRANSACTIONS ON ANTENNAS AND PROPAGATION*, and as an Associate Editor of the *IEEE ANTENNAS AND PROPAGATION SOCIETY NEWSLETTER*. In 1984, he received an NSF Presidential Young Investigator Award, as well as the "Keys to the Future" Award, from the IEEE Antennas and Propagation Society. In 1986, he received the R.W.P. King Best Paper Award from the IEEE Antennas and Propagation Society.